*Aust. J. Phys.*, 1975, **28**, 209–30

# 5 GHz Polarization Observations of 33 Galactic Radio Sources

*D. K. Milne*[A] *and J. R. Dickel*[B]

[A] Division of Radiophysics, CSIRO, P.O. Box 76, Epping, N.S.W. 2121.
[B] Department of Astronomy, University of Illinois at Urbana-Champaign, Urbana, Illinois 61801, U.S.A.

*Abstract*

Polarization observations have been made of 33 galactic radio sources, mostly supernova remnants, at a frequency of 5 GHz using the 64 m telescope at Parkes. Maps of the observed polarization vectors superposed upon total intensity isotherms are presented for each source.

## Introduction

Over the past few years we have used the CSIRO 64 m radio telescope at Parkes to systematically map the 2·7 GHz linearly polarized radio emission from 24 galactic radio sources thought to be supernova remnants (SNRs) (Milne 1968, 1971*a*, 1972; Milne and Dickel 1971, 1974). In the present paper we report a continuation of this investigation in which 5 GHz observations have been made of 33 objects, mostly SNRs, 18 of which are in common with the 2·7 GHz observations. In a later paper we will compare the two-frequency observations for these 18 sources to obtain magnetic field directions, Faraday rotation measures and depolarization distributions over the sources.

## Observations

A 5 GHz cryogenic parametric amplifier was used, switching between two orthogonal linearly polarized probes in a circular feed horn which under-illuminated the dish to reduce spillover effects; the half-power beamwidth was 4′·4 arc. The system noise temperature was 80 K over a 500 MHz band. Full-beam brightness temperature calibration was determined from scans of the small-diameter source Hydra A, for which an integrated flux density of 13·0 Jy* was assumed. The ratio of beam brightness temperature to flux density for a point source in this beam is 0·72.

To relate the total-power beam temperature $T_b$ to the polarization beam temperature $T_b^p$, a modulated noise signal simulating 100% linear polarization was injected after the RF switch. We have followed the recommendations of the working group on polarization for the IAU Commission 40 (XV General Assembly, Sydney 1973) and resolved the controversial factor of 2 in the specification of $T_b^p$ so that the degree of polarization is given by $T_b^p/T_b$.

The general method of observation has been described by Milne (1972) and by Milne and Dickel (1974); it involved scans with the telescope feed set successively at position angles (PA) of 0°, 45°, 90° and 135°. The signal recorded at a given PA

* 1 jansky (Jy) = $10^{-26}$ W m$^{-2}$ Hz$^{-1}$.

is the difference between the signal with $E$ vector at that PA minus the signal with $E$ vector at PA+90°. Thus the observing procedure is, in principle, redundant in that the signal $S_0$ recorded at a PA of 0° is opposite and equal to $S_{90}$ at 90°, i.e.

$$S_0 = (I_0 - I_{90}) \quad \text{and} \quad S_{90} = (I_{90} - I_0).$$

However, in practice there is generally some difference in the response of the two probes which is cancelled by taking the difference between these orthogonal outputs. The two linear Stokes parameters $Q$ and $U$ are then given by

$$Q = \tfrac{1}{2}(S_0 - S_{90}) \quad \text{and} \quad U = \tfrac{1}{2}(S_{45} - S_{135}).$$

These are combined to yield the magnitude $(Q^2+U^2)^{\frac{1}{2}}$ and direction $\frac{1}{2}\arctan(U/Q)$ of the polarization $E$ vectors. The total intensity Stokes parameter $I$ is the sum of the outputs from the two orthogonal feeds, i.e. the total power output before phase detection, and this was averaged over the four scans in each set.

The procedure was to scan at 1° $\text{min}^{-1}$, generally in declination, across the source at each of the four PA for fixed right ascensions separated by approximately 2′ arc. The two receiver outputs (switched and total power) were sampled every 2″ arc with a 30 ms time constant and averaged over 2′ arc intervals along each scan, to provide a 2′ × 2′ arc data grid. For a few of the weaker sources several sets of such data were integrated to improve the sensitivity. Typical noise levels were such that polarization temperatures of ~0·03 K could be detected in a single set of observations.

Level baselines were then fitted to the same section of each of the four scans of a set, thus minimizing each of the Stokes parameters in this region. Generally the region of lowest total power brightness was chosen. For many sources we made additional polarization scans, in right ascension, to assist us in the choice of baselevel. Generally the procedure was simple and led to zero polarization off the source; in a few cases (e.g. Kes 40, CTB 37) we had considerable difficulty in fitting consistent baselevels. It should be noted that in general the polarization shown is not absolute and that a vector (constant over each field) could be added to each figure.

To determine the polarized emission from a radio source it is necessary to separate several instrumental effects from the observed response. The use of an altitude–azimuth mounted telescope makes this analysis possible, since the telescope polarization will remain fixed in direction with respect to the elevation axis of the dish whereas the linear polarization of the sky will appear to rotate through the range of the parallactic angle as the source moves across the sky. In our reduction program it is possible to make corrections in both feed angle (measured clockwise around the dish from the elevation axis) and position angle (measured in the usual convention of eastward from north in the sky) to correct for the various effects. We now consider each of these effects separately.

### (*a*) *Reflector Polarization*

Elliptical primary feed illumination combined with large-scale irregularities in the reflector surface may cause variation in antenna gain with change in feed orientation. An instrumental polarization will result which will remain fixed in feed angle and percentage at all azimuths but may change with zenith angle as the reflector distorts differentially under the varying effect of gravity. From observations of several unpolarized sources at various zenith angles this effect was found to be less than $\frac{1}{2}\%$ for the present observations.

(*b*) *Differential Gain in the Two Feed Probes*

This effect is evaluated by comparison of the two measurements in orthogonal directions which, as described above, should be of equal magnitudes but of opposite sign. No such effect was apparent in our observations, but if it had been present the use of both orthogonal differences would have averaged the gains in the two probes, thus cancelling the spurious polarization.

(*c*) *Misalignment of Phase Centre and Rotation Axis of Feed*

This defect will manifest itself with a period corresponding to a full 360° rotation of the feed rather than the 180° period for linear polarization. Therefore, checks of the source polarization (and positions) were made at 45° intervals through a full 360° for several sources. No variation with this period was apparent.

(*d*) *Beam Shape Imperfections*

In general there could be a switched response to unpolarized radiation off-axis which arises from differences in the details of the beam shape (including the side lobes) for the two switch positions. If the two beams are symmetrical, similar and orthogonal (e.g. two identical elliptical beams with their major axes orthogonal) then the spurious polarization is cancelled by taking the differences between orthogonal scans, as we have done. It should be noted that several authors (including the present ones) have in the past followed Davies and Gardner (1970) and have incorrectly stated that the spurious effect produced by beam ellipticity is proportional to the gradient of the total power brightness; it is in fact related to the second (and not the first) derivative of the sky brightness.

(*e*) *Cross-polarization Lobes*

In contrast to the preceding effects, this spurious polarization is a response to incident radiation which is *polarized* in the direction orthogonal to the polarization for which the beam is set. It arises from rotation of the plane of polarization on reflection by the intermediate segments of the telescope. For the hybrid-mode feeds used here, these cross-polarization lobes are at least 20 dB below the main beam, so that the maximum spurious polarization would only be 1% of the incident polarization—a negligible effect in any of the regions observed.

(*f*) *Galactic Background*

As seen in our work at 2·7 GHz (Milne 1972; Milne and Dickel 1974), the polarization of the galactic background is generally the most significant feature affecting the accuracy of the determination of the polarization of a source. Significant changes in the background polarization often occur on the scale of the size of an SNR and no unambiguous method is available to separate the source polarization from that of the background. This is also to be seen in several of the present maps, e.g. in CTB 37 (Fig. 9*b*).

The magnitude of the typical spurious effects can be gauged from Fig. 1*a*, which is a polarization and total-power map of the strong unpolarized source Hydra A. Spurious polarization (most likely due to effect (*d*) above) of about ½% of the peak temperature can be seen in this figure. This is a fairly small value and corrections have not been applied to any of the results given in this paper.

**Table 1. 5 GHz flux densities**

| Galactic source number | Source name | Total flux density (Jy) | Average polarization (%) | Figure number |
|---|---|---|---|---|
| | Hydra A | 13·0 | 0·3 | 1*a* |
| 184·6−5·8 | Taurus A | — | — | 1*b* |
| 188·9+3·0 | IC 443 | 70 | 3·6 | 1*c* |
| 260·5−3·3 | Puppis A | 65 | 3·1 | 1*d* |
| 284·2−1·8 | MSH 10−*53* | 6·1 | 5·0 | 2*a* |
| 290·1−0·8 | MSH 11−*61A* | 20·2 | 3·2 | 2*b* |
| 292·0+1·8 | MSH 11−*54* | 8·9 | 1·2 | 2*c* |
| 295·2−0·6 | Kes 16 | 26 | 0·4[A] | 2*d* |
| 296·5+9·7 | 1209−51/52 | 30 | 17·1 | 3 |
| 296·8−0·3 | 1156−62 | 5·5 | ~8 | 4*a* |
| 304·6+0·1 | Kes 17 | 6·9 | 1·3 | 4*b* |
| 308·7+0·0 | 1338−62 | 6·5 | 2·8 | 4*c* |
| 315·4−2·3 | MSH 14−*63* | 18·7 | 5·7 | 5*a, b* |
| 316·3+0·0 | MSH 14−*57* | 16·7 | 2·9 | 6*a* |
| 320·4−1·0 | MSH 15−*52* | 40 | 5·0 | 6*b* |
| 326·2−1·7 | MSH 15−*56* | 75 | 8·2 | 7*a* |
| 327·4+0·4 | Kes 27 | 8·2 | 7·6 | 7*b* |
| 327·6+14·5 | SN AD 1006 | 8·1 | 9·8 | 8*a* |
| 332·4+0·1 | Kes 32 | 11 | 3·9 | 8*b* |
| 337·3+1·0 | Kes 40 | 6·0 | 2·3 | 8*c, d* |
| 342·1+0·1 | MSH 16−*48* | 26·4 | 4·2 | 9*a* |
| 348·5+0·1 | CTB 37A | 43 | 2·9 | 9*b* |
| 348·7+0·3 | CTB 37B | 32 | | |
| 355·2+0·1 | NGC 6383 | 15·2 | — | 9*c* |
| 350·0−1·8 | 1724−38 | — | ~12[A] | 9*d* |
| 357·7−0·1 | MSH 17−*39* | 14·6 | 2·6 | 10*a* |
| 4·5+6·8 | Kepler's SNR | 6·8 | 1·3 | 10*b* |
| 5·3−1·1 | Milne 56 | 27 | 5·0 | 10*c* |
| 6·6−0·2 | W28 | 176 | 2·6 | 11*a* |
| 7·7−3·7 | 1814−24 | 6·7 | ~10 | 11*b* |
| 18·9+0·3 | Kes 67 | 18·5 | 3·1 | 11*c* |
| 21·8−0·6 | Kes 69 | 30 | 3·1 | 12*a* |
| 27·3+0·0 | Milne 62 | — | 2·2[A] | 12*b* |
| 39·2−0·3 | NRAO 593 | 8·8 | 3·0 | 12*c* |

[A] Over the portion of the source mapped in polarization.

**Figs 1–12** (pp. 213–24). Results of the survey showing the total-power contours and polarization vectors at 5 GHz for the unpolarized source Hydra A and the 33 galactic sources. The contour unit (CU), the linearly polarized beam brightness temperature scale and the half-power beam size (B) are indicated on each map.

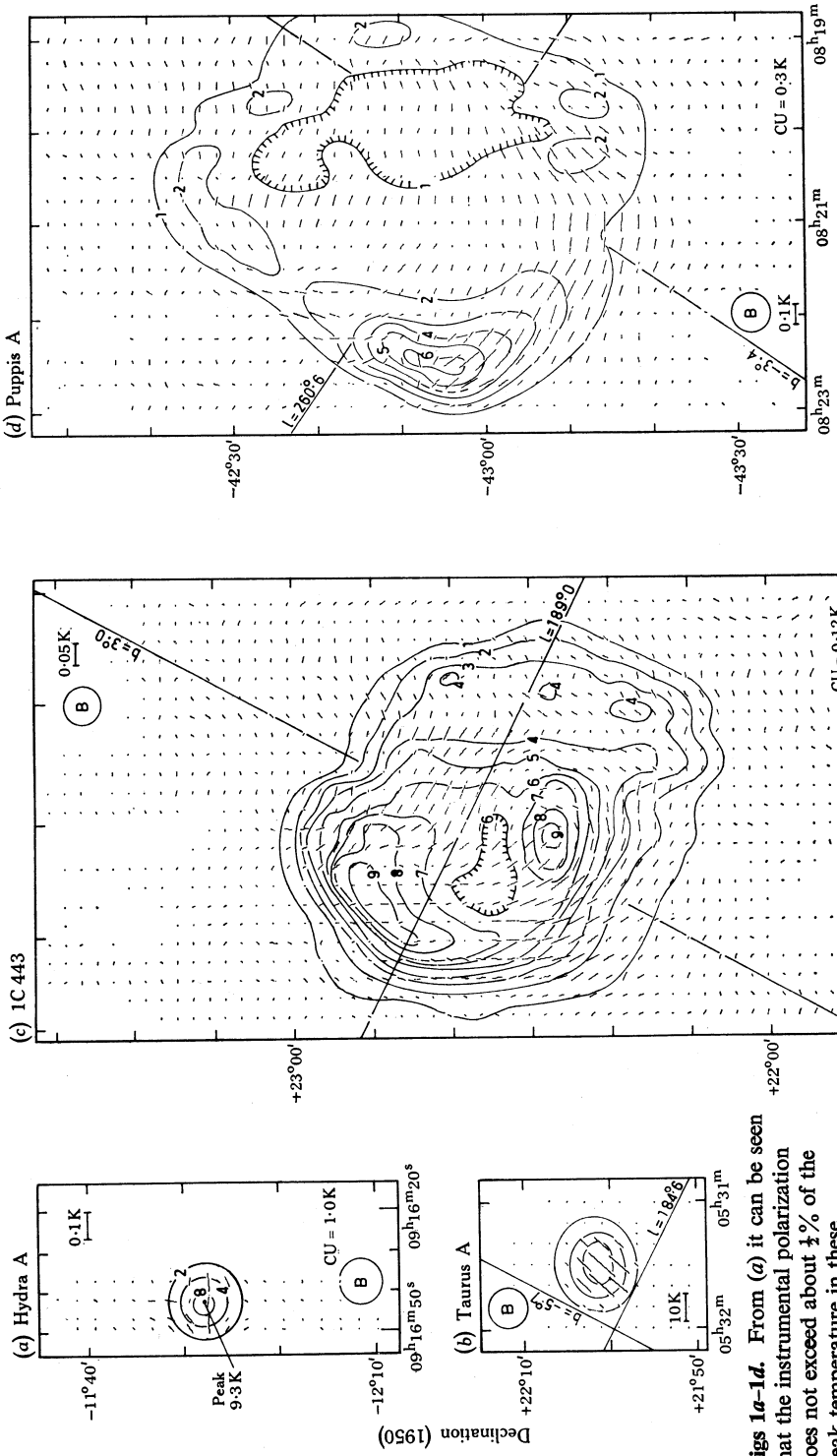


**Figs 1*a*–1*d*.** From (*a*) it can be seen that the instrumental polarization does not exceed about ½% of the peak temperature in these observations. For (*b*) the unlabelled contours show only the source position (see text).

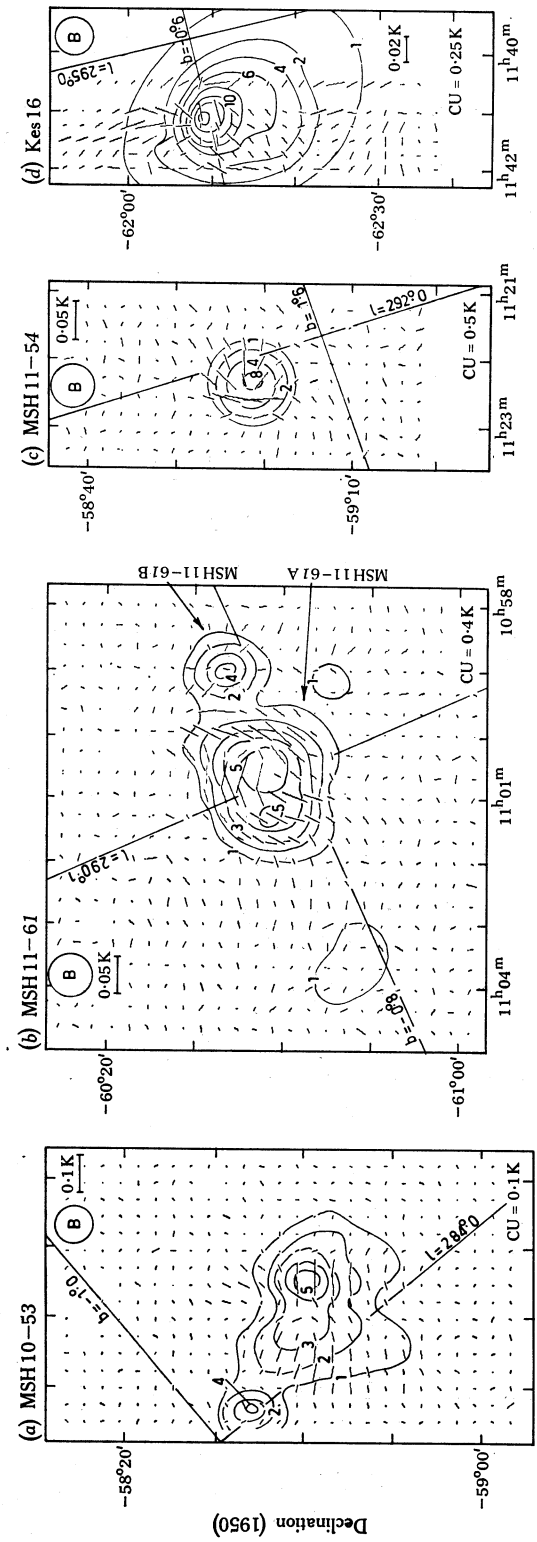
(a) MSH10−53
(b) MSH11−61
(c) MSH11−54
(d) Kes16
MSH11−61A
MSH11−61B
Declination (1950)
Right ascension (1950)

**Figs 2a–2d**

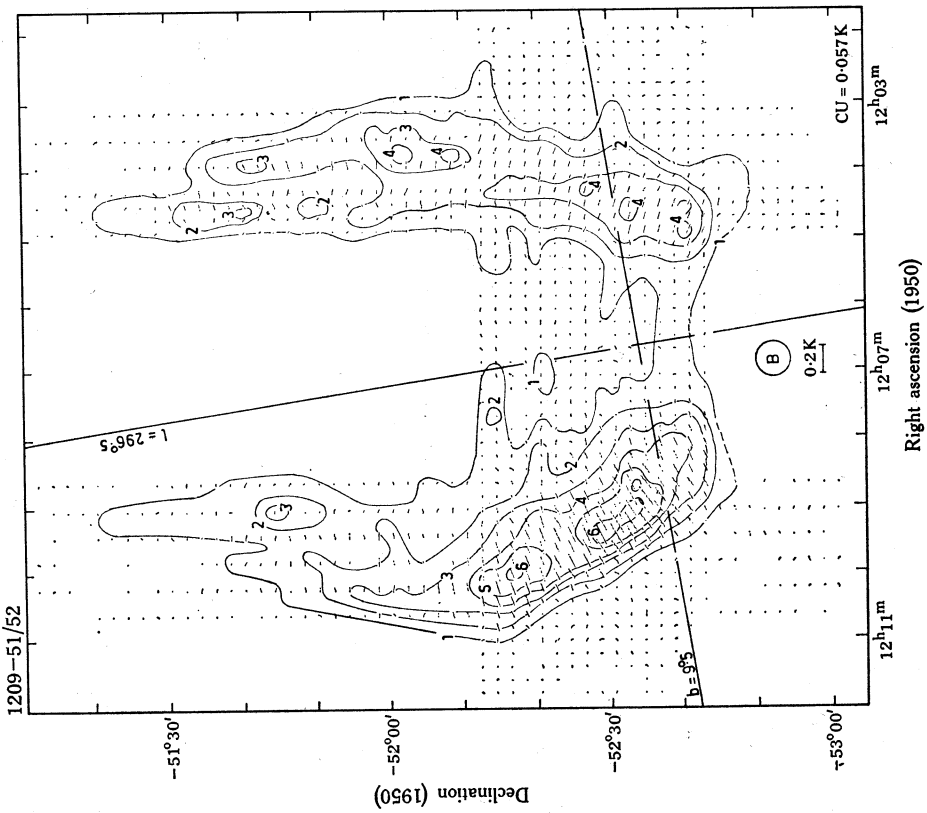
1209−51/52
l = 296°5
b = 9°5
CU = 0·057 K
B
0·2 K
−51°30′
−52°00′
−52°30′
−53°00′
Declination (1950)
12h11m
12h07m
12h03m
Right ascension (1950)

Fig. 3

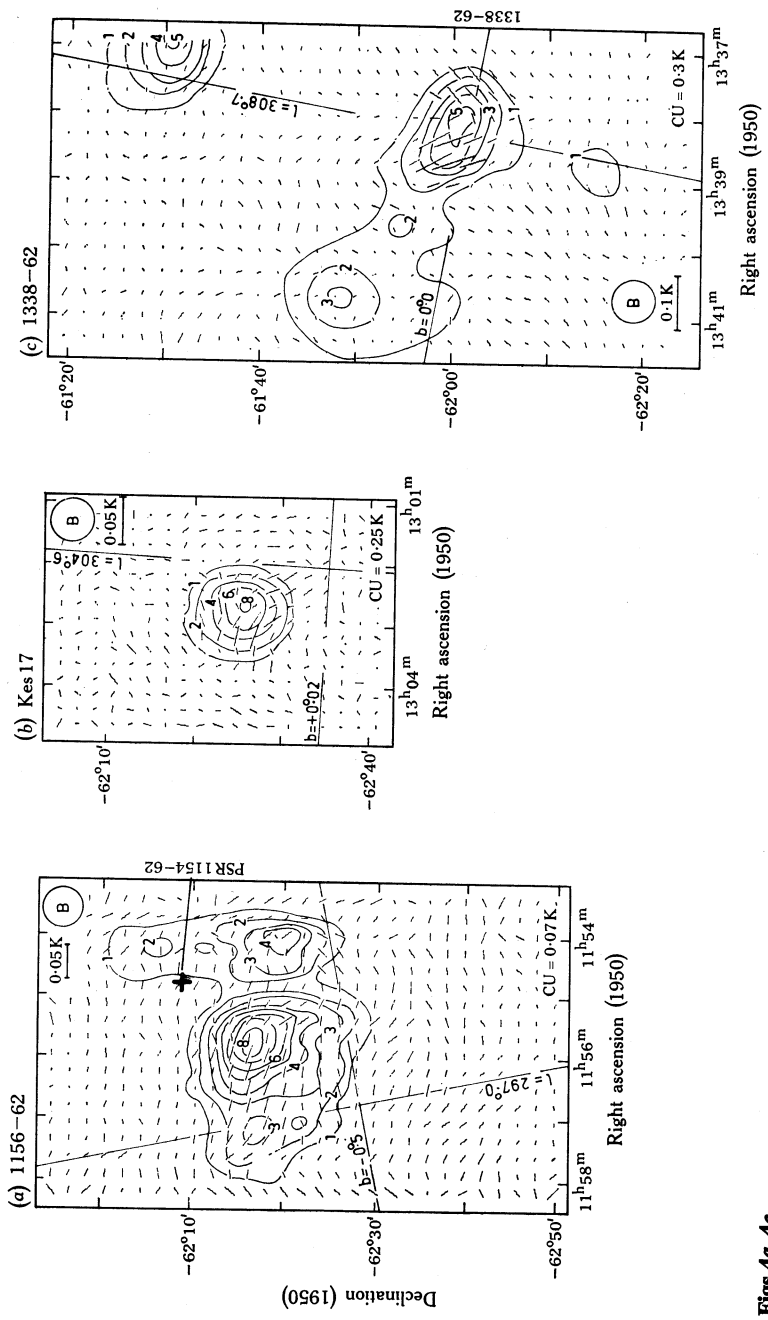
(a) 1156−62
PSR 1154−62
B
0·05K
CU = 0·07K
l = 297°0
b = −0°5
−62°10′
−62°30′
−62°50′
11h58m
11h56m
11h54m
Right ascension (1950)
Declination (1950)
(b) Kes 17
B
0·05K
CU = 0·25K
l = 304°6
b = +0°2
−62°10′
−62°40′
13h04m
13h01m
Right ascension (1950)
(c) 1338−62
1338−62
l = 308°7
b = 0°0
B
0·1K
CU = 0·3K
−61°20′
−61°40′
−62°00′
−62°20′
13h41m
13h39m
13h37m
Right ascension (1950)

**Figs 4a–4c**

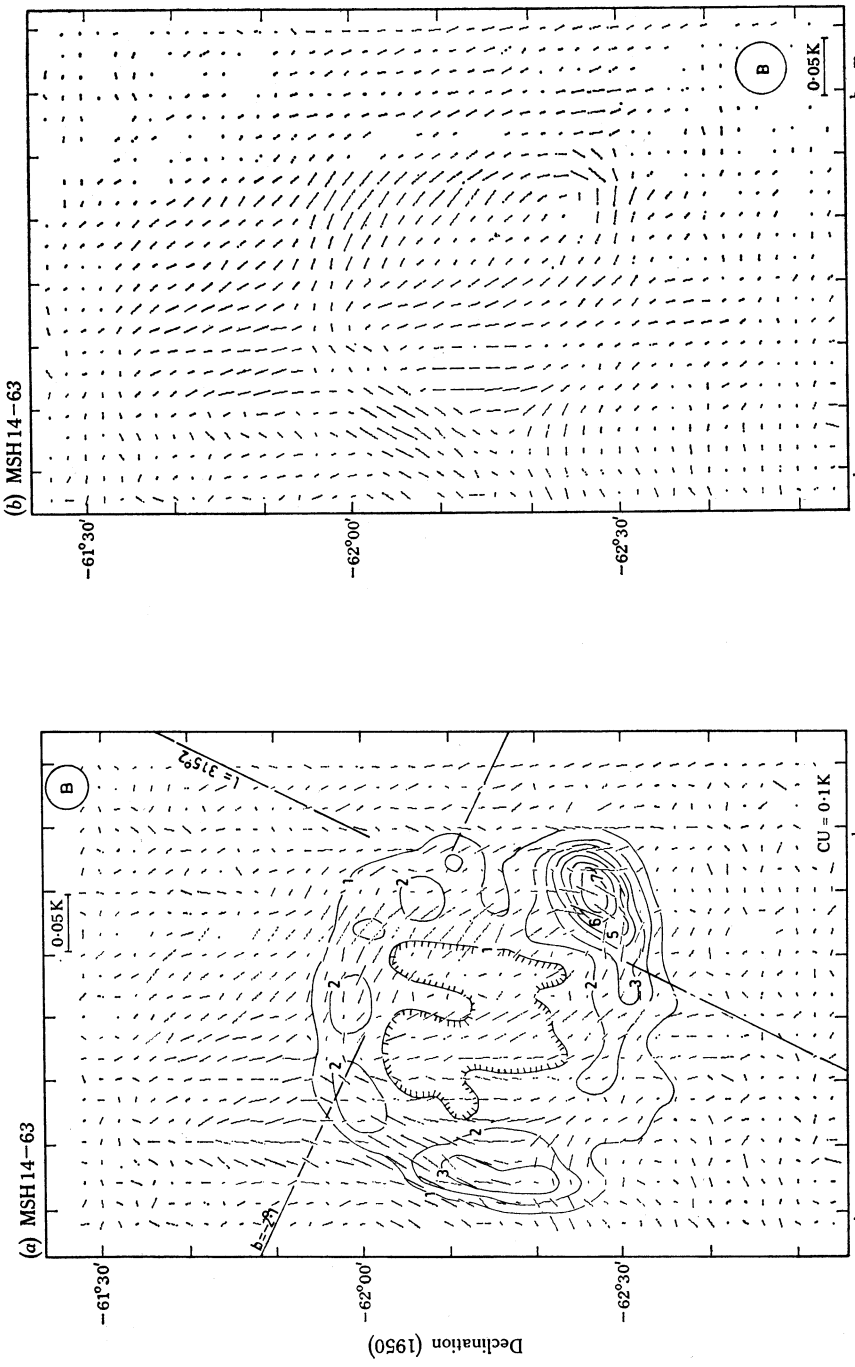


**Figs 5a, b.** A smoothed version of (*a*) is shown in (*b*) to better illustrate the general polarization distribution. The plotted vectors have been convolved to represent those which would have been observed by a telescope with a half-power beamwidth of 5′ arc.

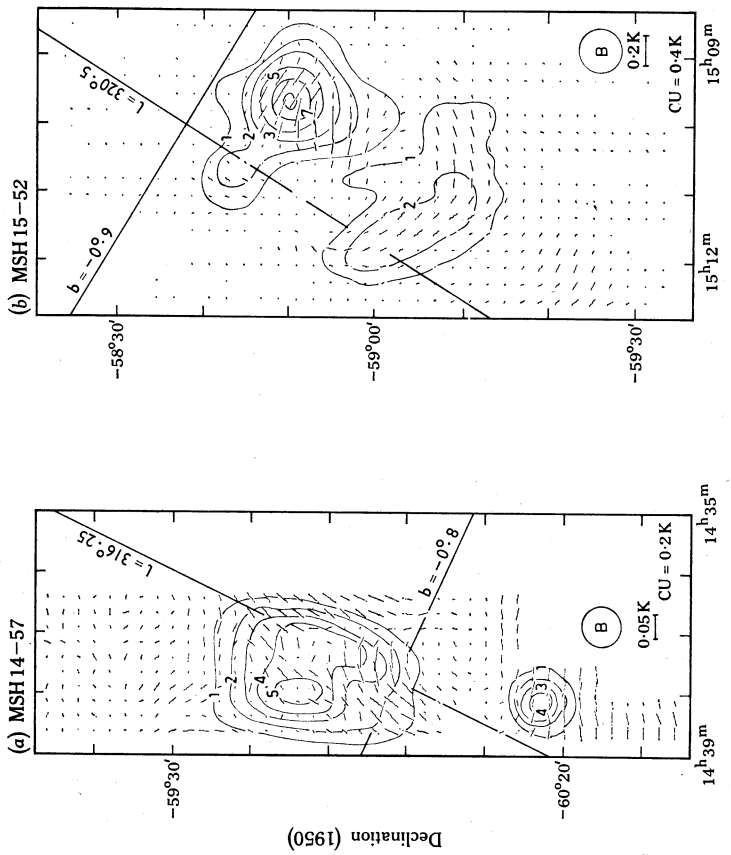
(a) MSH 14−57
(b) MSH 15−52
l = 316°.25
b = −0°.8
l = 320°.5
b = −0°.9
B
0·05K
CU = 0·2K
0·2K
CU = 0·4K
−59°30′
−60°20′
−58°30′
−59°00′
−59°30′
14h39m
14h35m
15h12m
15h09m
Declination (1950)
Right ascension (1950)

**Figs 6a, b**

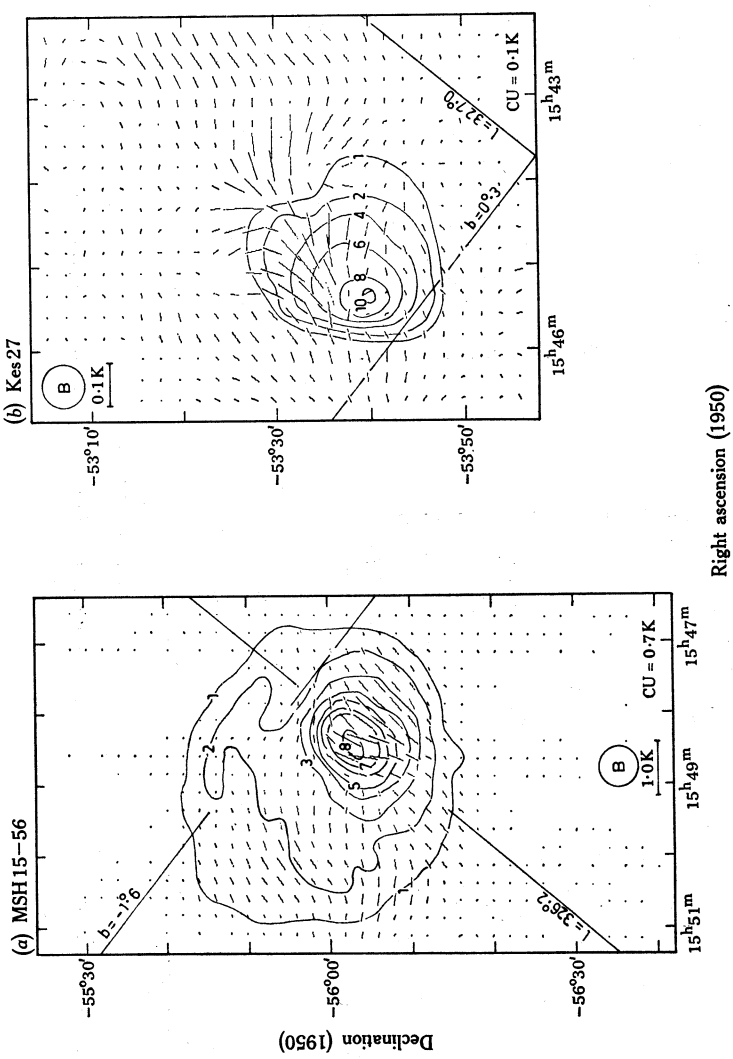
(a) MSH15−56
(b) Kes27
B
1·0K
0·1K
CU = 0·7K
CU = 0·1K
b = −1°6
b = 0°3
l = 326°2
l = 327°0
−55°30′
−56°00′
−56°30′
−53°10′
−53°30′
−53°50′
15h51m
15h49m
15h47m
15h46m
15h43m
Declination (1950)
Right ascension (1950)

Figs 7a, b

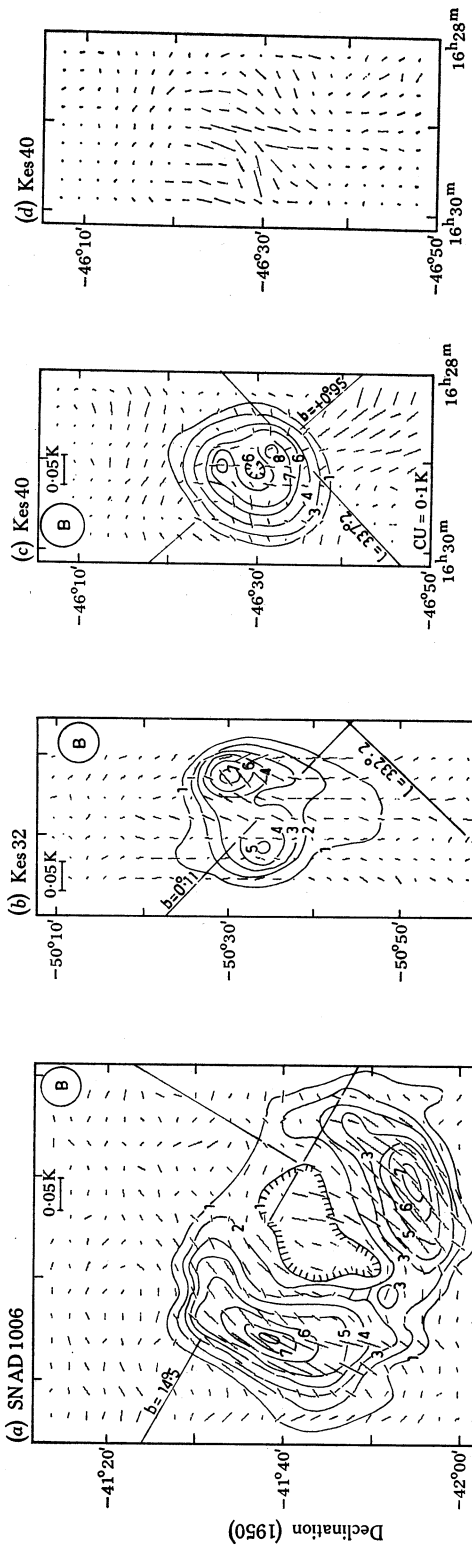


**Figs 8a, b.** In (*d*) an attempt has been made to separate the polarization of Kes 40 from that of the background by force-fitting zero polarization off the source at both ends of each scan.

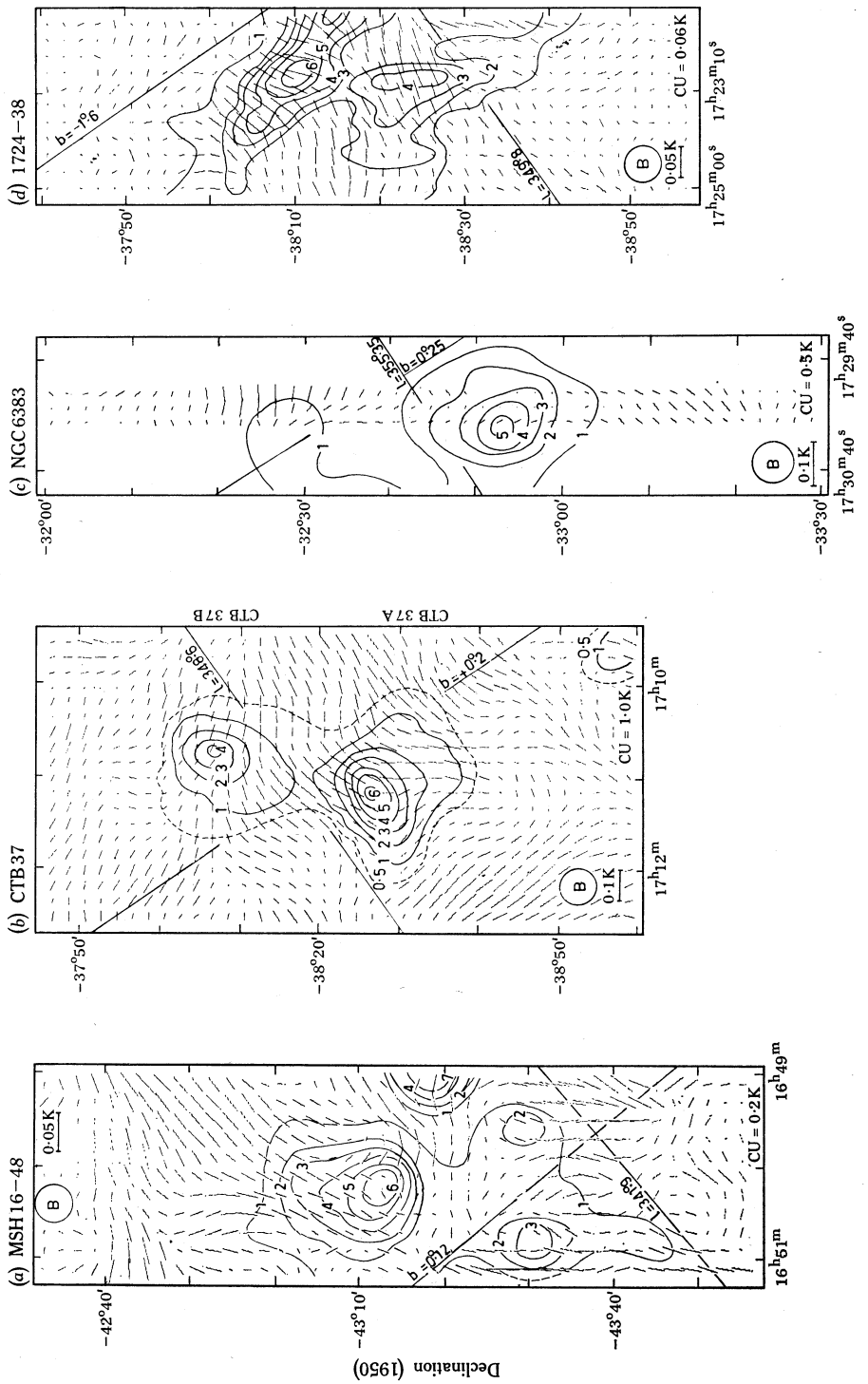
(a) MSH16−48
(b) CTB37
(c) NGC6383
(d) 1724−38
CTB 37A
CTB 37B
Declination (1950)
Right ascension (1950)

Figs 9a–9d

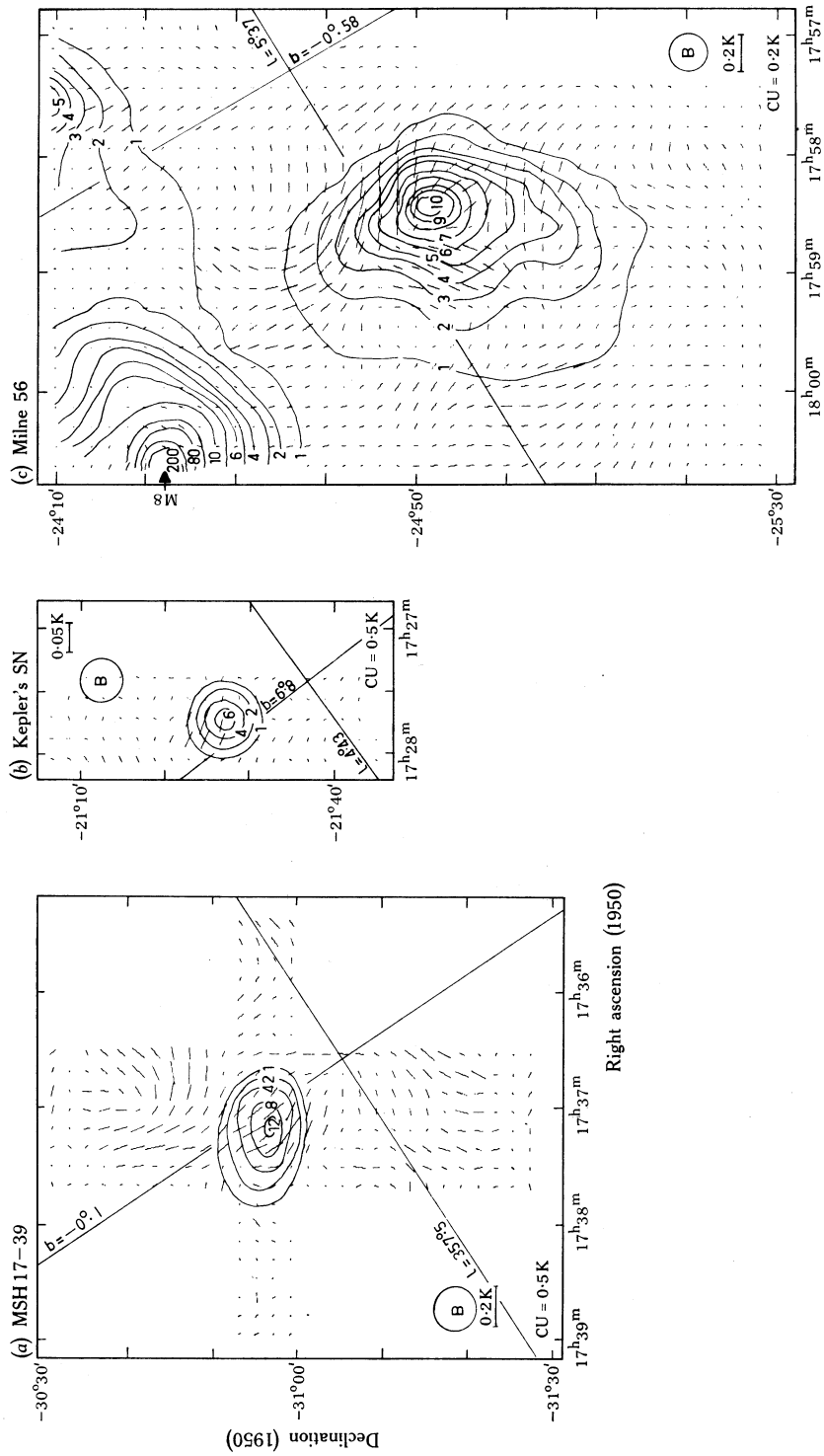


**Figs 10*a*–10*c*.** Note in (*c*) the very low instrumental polarization in the direction of the strong thermal source M8.

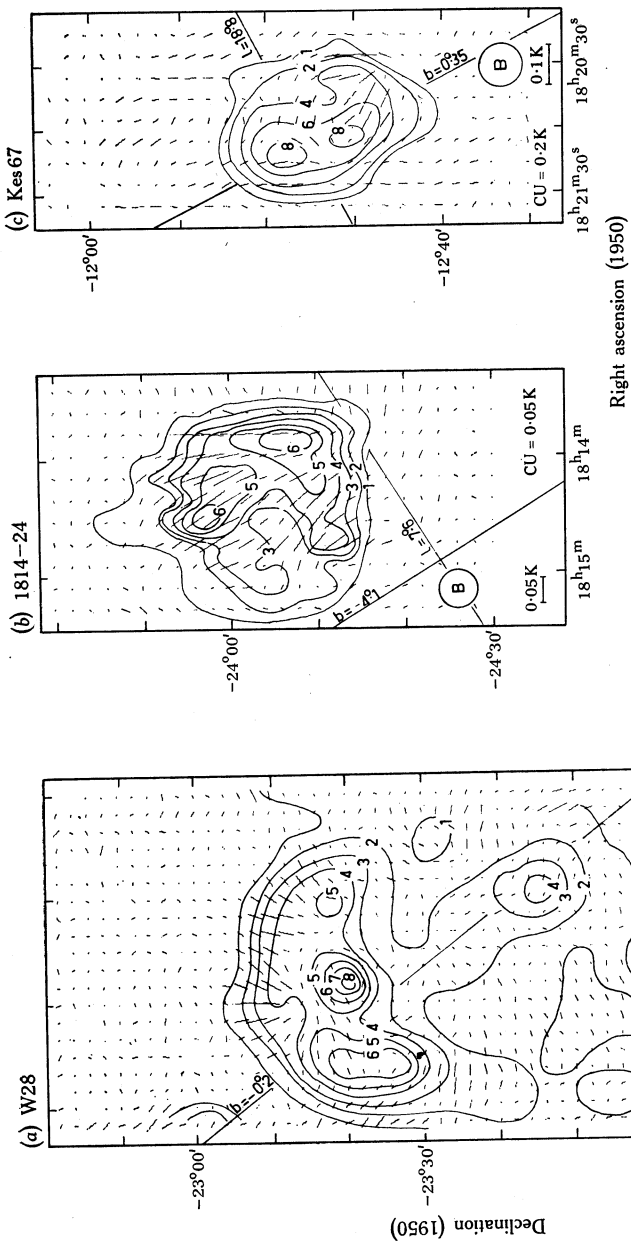
(a) W28
(b) 1814–24
(c) Kes 67
Declination (1950)
Right ascension (1950)
Right ascension (1950)
CU = 0·5K
CU = 0·05K
CU = 0·2K
0·2K
0·05K
0·1K
B

**Figs 11a–11c**

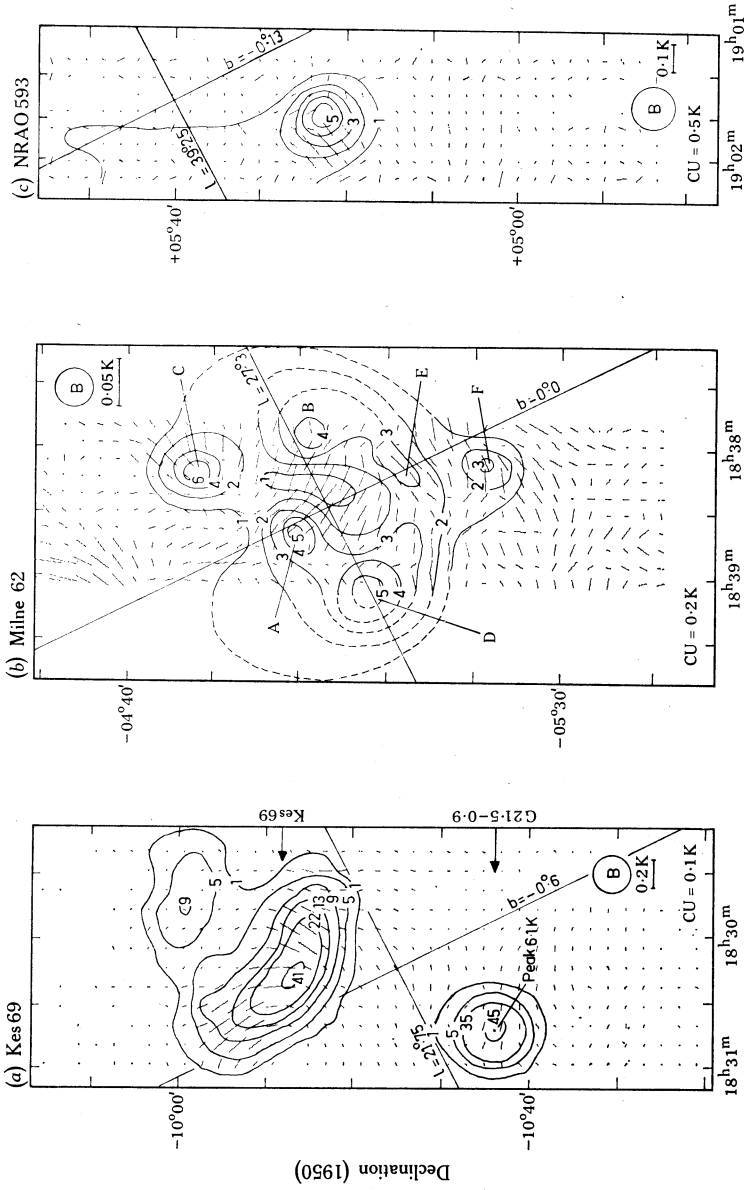
(a) Kes 69
(b) Milne 62
(c) NRAO 593
Declination (1950)
Right ascension (1950)
Kes 69
G21·5–0·9
Peak 61K
CU = 0·1K
CU = 0·2K
CU = 0·5K
0·2K
0·05K
0·1K
b = –0°·9
b = –0°·0
b = –0°·13
l = 21°·5
l = 21°·3
l = 28°·15
–10°00′
–10°40′
–04°40′
–05°30′
+05°40′
+05°00′
18h31m
18h30m
18h39m
18h38m
19h02m
19h01m

**Figs 12*a*–12*c***

**Results**

In Figs 1–12 we present the results of the survey in the form of maps of the total-power intensities on which have been superimposed polarization vectors (indicating the direction of the ***E*** vectors of the linearly polarized beam brightness and the magnitude of this brightness). In Table 1 we list the sources which were observed at 5 GHz and the integrated flux density of each derived from the total-power contours. The average percentage polarization for each source, which is also given, was derived by integrating the *magnitude* of the polarized flux density over the same area as that covered by the total-power contours and then dividing by the integrated flux density. It is therefore an intensity-weighted average and should not be seriously affected by random noise and background effects near the faint edges of the sources. Note that this is not the percentage polarization that would be seen with a beam very much larger than the angular size of the source. A brief discussion of each source follows.

*Tau A, G184·6−5·8 (Fig. 1b)*

This source was not resolved with our 4′·4 arc beam but has been from high-resolution observations (Wilson 1972); however, the polarization is uniformly directed over the source so that our measurement is meaningful as a PA calibration. The direction we obtain, a PA of 153°, is close to the values obtained by other workers (Hobbs and Haddock 1967; Sastry *et al.* 1967). For this very bright source the total-power amplifier was saturated so that the total power contours shown in Fig. 1*b* are distorted and hence are not labelled.

*IC 443, G188·9+3·0 (Fig. 1c)*

This distribution of polarization is very similar to that obtained by Kundu and Velusamy (1969) at 5 GHz (6′ arc beam) and by Milne and Dickel (1974) at 2·7 GHz (8′·4 arc) with a lower resolution.

*Puppis A, G260·5−3·3 (Fig. 1d)*

The shell structure of this source is obvious in the polarization distribution, as well as in the total-power contours.

*MSH 10−53, G284·2−1·8 (Fig. 2a)*

This weak source, which lies just to the south of the extended complex RCW 48 (Milne and Dickel 1974), exhibits definite polarization with a rather uniform orientation of the electric vectors. The small-diameter source seen on the east at $10^h 17^m 20^s$ and $-58° 34'$ has a much lower polarization. Since its peak brightness is progressively less at 2·7 GHz (Milne 1972) and at 408 MHz (Caswell and Clark 1975), it may be a (unassociated) thermal source.

*MSH 11−61, G290·1−0·8 (Fig. 2b)*

The eastern component (MSH 11−61A) is nonthermal (Milne 1969) and we see definite associated polarization, whilst the unrelated thermal source (MSH 11−61B) to the west (which is at a different distance; Dickel 1973*a*) shows little more than a slight increase over the background noise.

*MSH 11−54, G292·0+1·8 (Fig. 2c)*

This source has angular diameters of 3′·1 arc in right ascension and 3′·5 arc in declination (Dickel *et al.* 1973) and consequently is not resolved by our 4′·4 arc beam. The polarization shown in Fig. 2*c* has a maximum of only 1% of the peak source temperature and is therefore only twice the spurious polarization shown in Fig. 1*a* for Hydra A, although the polarization directions are different in these two cases. Higher resolution is needed to show meaningful polarization for MSH 11−54.

*Kes 16, G295·2−0·6 (Fig. 2d)*

Originally thought to be nonthermal (Kesteven 1968), this source has now been shown to have a thermal spectrum (Dickel *et al.* 1973) and to emit an H109$\alpha$ recombination line (Dickel and Milne 1972). The partial polarization map shown here does not show any features in the polarization that we could associate with Kes 16.

*1209−51/52, G296·5+9·7 (Fig. 3)*

This is the 'shell' source in Centaurus which was shown to have a well-defined circumferential magnetic field by Whiteoak and Gardner (1968). Because of the large extent of the source we did not map the whole area (as indicated by the pattern of polarization vectors in the figure). Our increased resolution provides a little more total-power detail than was shown by the Whiteoak and Gardner map at 2·65 GHz. The polarization directions are very close to those at 2·65 GHz, confirming the extremely small Faraday rotation measures (of only a few tens of radians per square metre found by Whiteoak and Gardner). We also confirm that the magnetic field direction is 'tangential'.

*1156−62, G296·8−0·3 (Fig. 4a)*

The shell structure of this source, clearly evident on the 408 MHz map of Large and Vaughan (1972), is not as obvious on the present map, made with similar resolution. We also resolve a distinct source to the west at R.A. $11^h\,54^m$ and Dec. −62° 20′ which was evident as a bulge on the 2700 MHz contours made with lesser resolution by Milne and Dickel (1974). Although there is polarization in this direction there is little that one could associate with the SNR. The flux density measured here is consistent with the values quoted by Large and Vaughan, Milne and Dickel, and Caswell *et al.* (1975) for a spectral index of −0·5.

*Kes 17, G304·6+0·1 (Fig. 4b)*

The polarization in the direction of this unresolved source is only about 1½% of the peak intensity, but it is thought that the increased polarization is associated with Kes 17.

*1338−62, G308·7+0·0 (Fig. 4c)*

Suggested by Clark *et al.* (1973) as a supernova remnant, the source 1338−62 lies at the extreme western end of the extended region running east–west through the centre of Fig. 4*c*. The maximum polarization here is in excess of 5% of the peak temperature and would seem to be definitely associated with the SNR.

*MSH 14−63, G315·4−2·3 (Fig. 5)*

Polarization maps at 2·7 and 1·41 GHz have been published by Milne (1972) for this relatively large shell source of low surface brightness. The data in Fig. 5*a*

suggest consistent polarization around the shell of this source, which is somewhat greater than the background polarization to the north. This pattern of polarization is more easily seen in Fig. 5*b*, where we have smoothed the original data from Fig. 5*a* with a gaussian filter to an effective resolution of 5′ arc.

*MSH 14−57, G316·3+0·0 (Fig. 6a)*

In this field we see substantial polarization well off the SNR. The source to the south, G316·4−0·4, has a thermal spectrum (from comparison with the 408 MHz data of Shaver and Goss 1970) and the polarization in this direction is apparently part of an extended background.

*MSH 15−52, G320·4−1·0 (Fig. 6b)*

This source has the peripheral brightness distribution commonly found in supernova remnants. The distinct northern peak is coincident with the emission nebula RCW 89 and the X-ray source 2U 1509−58 (Giacconi *et al.* 1972), contrary to the comment by van den Bergh *et al.* (1973).

*MSH 15−56, G326·2−1·7 (Fig. 7a)*

This region contains a high surface brightness source centred towards the south-west of a low brightness plateau which shows a marked 'shell structure' at 408 MHz (Clark *et al.* 1975). This 'shell' is barely discernible in our total-power contours and presumably has a steeper spectrum than other parts of the source. Certainly there is a substantial difference between the spectral index of the bright inner prominence ($\alpha \approx -0{\cdot}1$) and the plateau ($\alpha \approx -0{\cdot}4$) (Clark *et al.* 1975), and one would be tempted to say that there was a chance superposition of two sources in this direction. However, the high degree of polarization over both the plateau and this prominence in Fig. 7*a* suggests a physical association between the two features. A 5 GHz polarization map made by Whiteoak and Gardner (1971) using the Parkes 64 m telescope shows essentially the same distribution of total power and polarization as our map.

*Kes 27, G327·4+0·4 (Fig. 7b)*

This field shows quite high systematic polarization away from the source Kes 27. The polarization on the source seems to be a continuation (and intensification) of this background polarization.

*SN AD 1006, G327·6+14·5 (Fig. 8a)*

This map of the polarization vectors at 5 GHz complements the preliminary work of Milne (1971*b*) at that frequency and corresponds closely to his map at 2·7 GHz. AD 1006 clearly has small Faraday rotation and a radial magnetic field.

*Kes 32, G332·4+0·1 (Fig. 8b)*

The western peak of this source is polarized well above the noise level. The sudden rotation of the ***E*** vector direction between the two most westerly scans is in fact real, as confirmed by additional scans made to resolve this apparent contradiction.

*Kes 40, G337·3+1·0 (Figs 8c, d)*

This circularly shaped SNR seems to be only weakly polarized compared with the region to the south in Fig. 8*c*, in agreement with our results at 2·7 GHz (Milne and Dickel 1974). We have therefore attempted in Fig. 8*d* to remove the background

polarization by fitting sloping linear baselevels to give an approximate indication of the weak polarization on Kes 40 itself.

*MSH 16−48, G342·1+0·1 (Fig. 9a)*

This complex covering an area about 40′ arc in diameter north of MSH 16−48 (Thomas and Day 1969) and only partially shown in our observations was suggested as an SNR by Kesteven (1968), although it is now thought that the sources in the complex have thermal spectra (Caswell and Clark 1975). In the present study we see polarization in this field but we cannot associated it with any particular features in the total-power map.

*CTB 37A, B; G348·5+0·1, G348·7+0·3 (Fig. 9b)*

It is impossible to recognize the polarization of either of the distinct SNRs against the very bright and variable polarization of the galactic background. With higher resolution, the southern source, CTB 37A, shows a definite shell on the north-east side contrasted with a more diffuse structure on the south-west (Dickel *et al.* 1973), but there is no apparent orientation or change in intensity of the polarization vectors to match this structure.

*NGC 6383, G355·2+0·1 (Fig. 9c)*

This source was once thought to be nonthermal (Reifenstein *et al.* 1970). Dickel and Milne (1972) have since found a relatively strong hydrogen recombination line in this direction, and a thermal spectrum is derived from the present flux density and the flux densities given by Milne *et al.* (1969). The three polarization scans only that were made do show results but the polarization is not related to the continuum source.

*1724−38, G350·0−1·8 (Fig. 9d)*

Our map covers only part of the bright arc comprising the main shell of this source, which was first identified as an SNR by Clark *et al.* (1973). There is strong polarization in the part of the shell covered in this work.

*MSH 17−39, G357·7−0·1 (Fig. 10a)*

This source, very near the galactic centre, is situated on a strong background which is significantly polarized. There is a definite increase in the polarized intensity at the position of the source but it is difficult to completely accept this as being associated with the SNR. A 5 GHz polarization map of this object given by Kundu *et al.* (1974) does not show the extensive polarization away from the source, and they do not describe its removal. Their polarization distribution over the source differs considerably from ours.

*Kepler's SNR, G4·5+6·8 (Fig. 10b)*

Although unresolved with our 4′·4 arc beam, this bright young SNR does have a net polarization at 5 GHz of about 1·5%.

*Milne 56, G5·3−1·1 (Fig. 10c)*

The original polarimetric map of this source published previously (Milne and Dickel 1971) is given again here for completeness as Fig. 10*c*. There is strong polarization in the direction of Milne 56, with a well-ordered change in orientation of the electric vectors across the source. This matches well with the total-power outline, which has a sharp edge on the west side and then tails off eastward as if the expansion

were being retarded by denser cold gas to the west. The very bright HII region M8 appears on the north-east side of this map and the extremely small polarization observed in this direction further illustrates the negligible instrumental effects.

*W28, G6·6−0·2 (Fig. 11a)*

The distribution of polarization shown here completes that published for the brighter peaks by Milne and Wilson (1971) and is generally similar to the lower resolution map by Kundu (1970). Differences do occur, however, in that we do not find polarization to the north of W28. There is definite polarization around the whole shell of the SNR.

*1814−24, G7·7−3·7 (Fig. 11b)*

This source with a well-defined shell structure (particularly on the west side) is strongly polarized over its whole extent. The orientation of the polarization vectors appears very uniform over the whole source in contrast to the large variation observed at 2·7 GHz (Milne and Dickel 1974). This implies significant differential Faraday rotation across the source.

*Kes 67, G18·9+0·3 (Fig. 11c)*

The concentration of polarization towards the south-western part of this source and the PA of the ***E*** vectors in this region are similar to those obtained at the same frequency but with lower resolution and sensitivity by Velusamy (1973), and are compatible with the 2·7 GHz polarization (Milne and Dickel 1974).

*Kes 69, G21·8−0·6 (Fig. 12a)*

The rather high polarization of this source has also been observed at 2·7 GHz by us (Milne and Dickel 1974) and at 10·6 GHz by Velusamy (1973). The slight increase in polarized intensity around the position of the small-diameter source G21·5−0·9 to the south of Kes 69 has been noted previously (Milne and Dickel 1974); the source has a very flat spectrum (Dickel 1973*b*) and its nature remains uncertain.

*Milne 62, G27·3+0·0 (Fig. 12b)*

The general structure of this source appears to be a shell with a number of individual peaks, designated A–F following Milne (1969) and Willis (1973). Recently Caswell and Clark (1975) have demonstrated that, with the exception of source A (4C −04·71, Kes 73), this complex has a thermal spectrum, and presumably the polarization seen here and at 2·7 GHz (Milne and Dickel 1974) is a galactic feature.

*NRAO 593, G39·2−0·3 (Fig. 12c)*

Clearly there is polarization associated with NRAO 593, but it is a small-diameter source and higher resolution observations are needed.

## Discussion

Looking collectively at the 5 GHz data given here, we reiterate one point which we have made before: that the polarization seemingly associated with the SNR in many cases is of the same order as that found away from the SNR. In a few cases one is tempted to suggest that the SNR polarization extends into the surrounding region, or that the background is compressed and enhanced by the SNR. However, there is no real evidence that the effect is any more than a chance superposition of the

SNR on the general galactic polarized emission. We will discuss the comparison between these maps and those at other frequencies, the derivation of the magnetic field direction, and the depolarization in a forthcoming paper.

**Acknowledgments**

We thank Allen Van Hoozen, Ralph Holmen and Andrew Hunt for help with the data analysis. This research was supported in part by the U.S. National Science Foundation Grant GP41560 to the University of Illinois.

**References**

van den Bergh, S., Marschen, A. P., and Terzian, Y. (1973). *Astrophys. J. Suppl. Ser.* **26**, 19.
Caswell, J. L., and Clark, D. H. (1975). Observations of radio sources formerly considered as possible supernova remnants. *Aust. J. Phys. Astrophys. Suppl.* No. 37 (in press).
Caswell, J. L., Clark, D. H., and Crawford, D. F. (1975). 408 and 5000 MHz observations of 12 probable supernova remnants. *Aust. J. Phys. Astrophys. Suppl.* No. 37 (in press).
Clark, D. H., Caswell, J. L., and Green, Anne J. (1973). *Nature (London)* **246**, 28.
Clark, D. H., Green, Anne J., and Caswell, J. L. (1975). Improved 408 MHz observations of some galactic supernova remnants. *Aust. J. Phys. Astrophys. Suppl.* No. 37 (in press).
Davies, R. D., and Gardner, F. F. (1970). *Aust. J. Phys.* **23**, 59.
Dickel, J. R. (1973*a*). *Astrophys. Lett.* **15**, 61.
Dickel, J. R. (1973*b*). *Aust. J. Phys.* **26**, 369.
Dickel, J. R., and Milne, D. K. (1972). *Aust. J. Phys.* **25**, 539.
Dickel, J. R., Milne, D. K., Kerr, A. R., and Ables, J. G. (1973). *Aust. J. Phys.* **26**, 379.
Giacconi, R., Murray, S., Gursky, H., and Kellog, E. (1972). *Astrophys. J.* **178**, 281.
Hobbs, R. W., and Haddock, F. T. (1967). *Astrophys. J.* **147**, 908.
Kesteven, M. J. L. (1968). *Aust. J. Phys.* **21**, 369.
Kundu, M. R. (1970). *Astrophys. J.* **162**, 17.
Kundu, M. R., and Velusamy, T. (1969). *Astrophys. J.* **155**, 807.
Kundu, M. R., Velusamy, T., and Hardee, P. E. (1974). *Astron. J.* **79**, 132.
Large, M. I., and Vaughan, A. E. (1972). *Nature (London) Phys. Sci.* **236**, 117.
Milne, D. K. (1968). *Aust. J. Phys.* **21**, 201.
Milne, D. K. (1969). *Aust. J. Phys.* **22**, 613.
Milne, D. K. (1971*a*). *Aust. J. Phys.* **24**, 429.
Milne, D. K. (1971*b*). *Aust. J. Phys.* **24**, 757.
Milne, D. K. (1972). *Aust. J. Phys.* **25**, 307.
Milne, D. K., and Dickel, J. R. (1971). *Nature (London)* **231**, 33.
Milne, D. K., and Dickel, J. R. (1974). *Aust. J. Phys.* **27**, 549.
Milne, D. K., and Wilson, T. L. (1971). *Astron. Astrophys.* **10**, 220.
Milne, D. K., Wilson, T. L., Gardner, F. F., and Mezger, P. G. (1969). *Astrophys. Lett.* **4**, 121.
Reifenstein, E. C., Wilson, T. L., Burke, B. F., Mezger, P. G., and Altenhoff, W. J. (1970). *Astron. Astrophys.* **4**, 357.
Sastry, Ch. V., Pauliny-Toth, I. I. K., and Kellermann, K. I. (1967). *Astron. J.* **72**, 230.
Shaver, P. A., and Goss, W. M. (1970). *Aust. J. Phys. Astrophys. Suppl.* No. 14, 77.
Thomas, B. M., and Day, G. A. (1969). *Aust. J. Phys. Astrophys. Suppl.* No. 11, 19.
Velusamy, T. (1973). Ph.D. Thesis, University of Maryland.
Whiteoak, J. B., and Gardner, F. F. (1968). *Astrophys. J.* **154**, 807.
Whiteoak, J. B., and Gardner, F. F. (1971). *Aust. J. Phys.* **24**, 913.
Willis, A. G. (1973). *Astron. Astrophys.* **26**, 237.
Wilson, A. S. (1972). *Mon. Notic. Roy. Astron. Soc.* **157**, 229.

Manuscript received 2 December 1974